Turing Patterning Using Gene Circuits with Gas-Induced Degradation of Quorum Sensing Molecules

Bartłomiej Borek[1,2], Jeff Hasty[1,2,3,4], Lev Tsimring[1,2]*

1 BioCircuits Institute, University of California San Diego, 9500 Gilman Dr., La Jolla, CA, 92037-0328, United States of America, 2 San Diego Center for Systems Biology, University of California San Diego, 9500 Gilman Dr., La Jolla, CA, 92037-0375, United States of America, 3 Department of Bioengineering, University of California San Diego, 9500 Gilman Dr., La Jolla, CA, 92037-0412, United States of America, 4 Molecular Biology Section, Division of Biological Sciences, University of California San Diego, 9500 Gilman Dr., La Jolla, CA, 92037-0116, United States of America

* ltsimring@ucsd.edu

Abstract

The Turing instability was proposed more than six decades ago as a mechanism leading to spatial patterning, but it has yet to be exploited in a synthetic biology setting. Here we characterize the Turing instability in a specific gene circuit that can be implemented *in vitro* or in populations of clonal cells producing short-range activator N-Acyl homoserine lactone (AHL) and long-range inhibitor hydrogen peroxide (H_2O_2) gas. Slowing the production rate of the AHL-degrading enzyme, AiiA, generates stable fixed states, limit cycle oscillations and Turing patterns. Further tuning of signaling parameters determines local robustness and controls the range of unstable wavenumbers in the patterning regime. These findings provide a roadmap for optimizing spatial patterns of gene expression based on familiar quorum and gas sensitive *E. coli* promoters. The circuit design and predictions may be useful for (re)programming spatial dynamics in synthetic and natural gene expression systems.

Introduction

Self-organization and self-assembly govern the emergent properties of spatial structures from the molecular to the galactic scale [1, 2]. In the nano-to-millimeter range chemical processes coordinate gene expression essential to the spatial organization of biological systems, including populations of microorganisms [3–6] and developing tissues [7–11].

One mechanism by which ensembles of cells could self-organize is the Turing instability [2, 12, 13] that occurs due to interplay of short-range activation and long-range inhibition. This instability then drives the formation of spatially periodic patterns. The Turing instability has been implicated in morphogenetic processes of amoebae [14], plants [15, 16], and animals [9, 10, 17–20]. The large number of unknown factors often makes it challenging to elucidate the essential determinants of morphogenesis in biological systems, but the instability has also been

directly engineered in low-component chemical reactions (malonic acid [21] and platinum surface [22]).

Despite the ubiquity of Turing patterns at the multi-cellular scale, they have yet to be demonstrated in gene expression sytems. This is surprising given the many alternative pattern forming mechanisms found in natural [3, 4, 6] and engineered [5, 6, 23–27] colonies of cells. For example, researchers have created gene circuits to produce stationary ring patterns in growing colonies of bacteria [5, 24, 28]. However, these stationary patterns required colony expansion and very particular initial conditions to form. Hsia *et* al. [29] have presented a theoretical model of a quenched oscillator circuit with one diffusible element that produces a Turing-like instability. There however, the temporal dynamics never settled to a stable fixed state due to persistent temporal oscillations. Another group [30] has recently developed a model of Turing pattern circuit using single promoter. However, even with common promoters, the activator and inhibitor genes would result in different production rate functions, especially if the compounds are to have largely differing diffusion rates. The lack of convincing examples raises the question of whether Turing patters can really be produced by genetic circuits.

If it is possible, then Turing patterning of gene expression could be quite useful for basic science and biotechnology applications. These include self-organized spatial sequestration of gene expression and downstream metabolites (as is currently done inside cells to improve yield [31]), spatially-patterned delivery of proteins [32], reprogrammed morphogenesis of cell populations [33], filtering of paracrine inputs from adjacent cells in populations [34], and chemical sensing [27]. Biosensing applications are particularly promising inasmuch as the Turing instability is inherently capable of amplifying small differences in initial conditions.

Motivated by this, we propose a realistic synthetic gene circuit that implements repressor-activated degradation using activating homoserine lactone and inhibitory peroxide gas, and demonstrate how this system can be switched between stable uniform states, limit cycles, and Turing patterns. We characterize the effects of experimentally relevant parameter changes on the presence and properties of the expected Turing patterns. We conclude by discussing our plans to experimentally implement the circuit and to refine the mathematical model that describes it.

Methods

The fixed points, eigenvalues and unstable wavenumbers of the differential equations were computed using the symbolic and variable-precision solvers in Matlab [35]. Bifurcation analysis was performed using the Matcont continuation package [36], and analysis of the Turing instability was performed as stated in the text, with a custom Matlab script. Spatio-temporal simulations were performed using custom Fortran code [37] using forward Euler with five point discretized Laplacian. Convergence of solutions was validated by simulating successively smaller spatial and temporal step sizes. For most cases we also tested both periodic and no-flux boundary conditions and used dx = 11.5 μm and dt = 10^{-5} min. We rescaled space by assuming $D_L = 5.6 \times 10^{-3}$ μm^2/min. S1 Table lists nominal parameter values used in the model equations.

Results

Turing pattern gene circuit with homoserine lactone and hydrogen peroxide gas

Based on our experience with using quorum-sensing signaling in synthetic circuit design [26, 27], we decided to use acyl homoserine lactone (AHL) as the short-range activator signal and
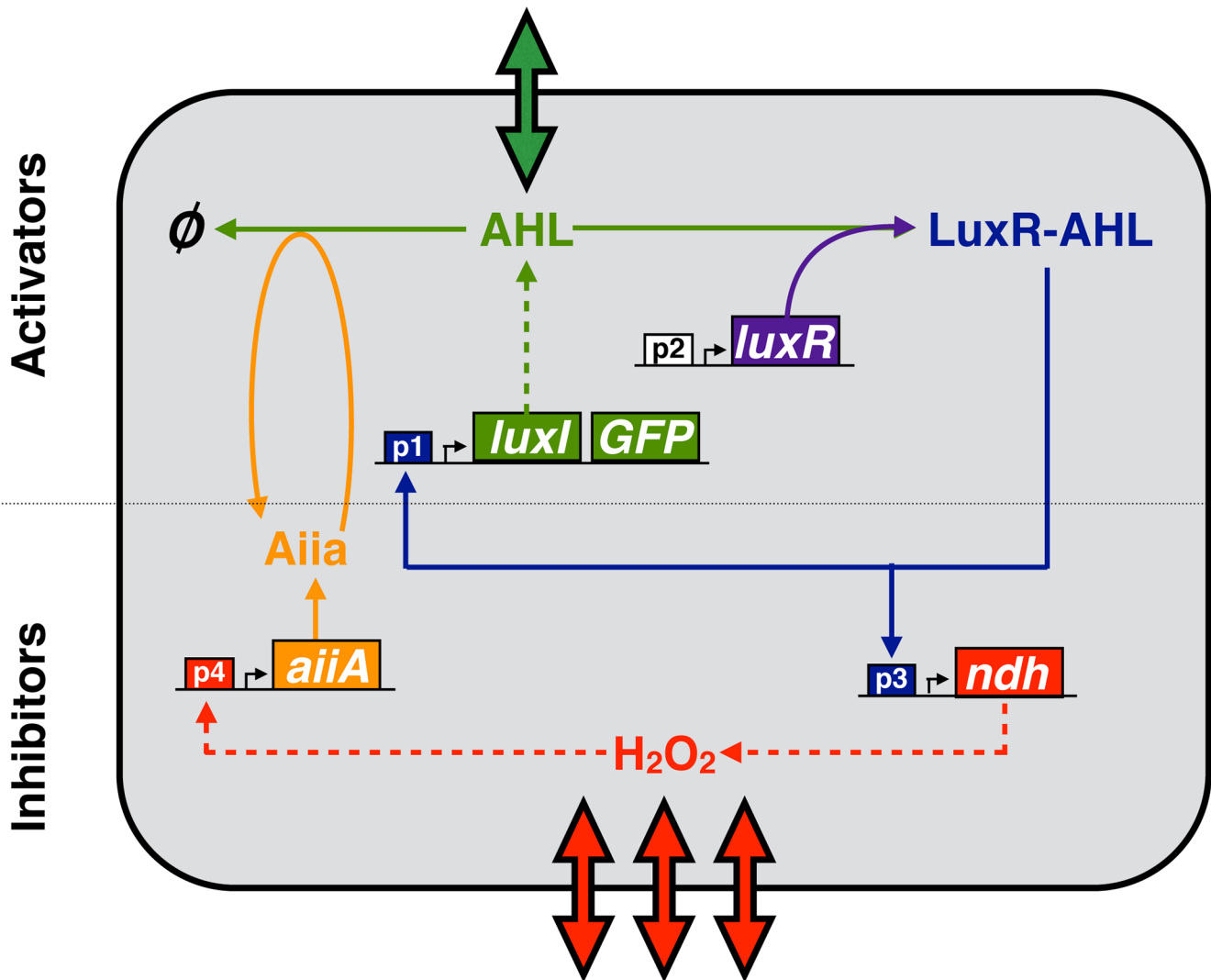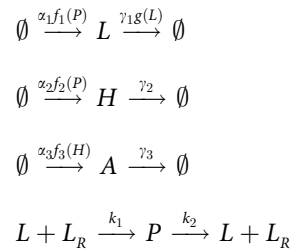
Fig 1. The proposed gene circuit for generation of Turing patterns. AHL activates its own production, but is degraded by Aiia. H_2O_2 is produced via the *ndh* gene, and activates the transcription of the *aiiA* gene. Intercellular transport and diffusion of AHL and H_2O_2 are represented by the thick arrows. The circuit is modeled by Eqs (1)–(4).

hydrogen peroxide gas (H_2O_2) as the long-range inhibitor signal (Fig 1). The choice to focus on a pure activator-inhibitor system [38] (where the activator self-activates and inhibitor self-inhibits) was based on the fact that the AHL quorum sensing system has a native positive feedback, and H_2O_2 does not. Several of the circuit components presented in Fig 1 have already been used to construct gene circuits that produced sustained temporal oscillations of fluorescent proteins [27]. The synthase LuxI produces AHL, and the Ndh protein generates H_2O_2. AHL binds with LuxR and activates the p_{lux}-like promoters (p_1 and p_2 in Fig 1). The *luxR* promoter (p_3 in Fig 1) is constitutive (unregulated). Controlled degradation of AHL is mediated by the AHL-lactonase, AiiA [39]. The *aiiA* gene can be activated by H_2O_2 by putting it under the control of a promoter (p_4 in Fig 1) such as: p_{topA}, which responds to H_2O_2 via the Fis pathway [40], or a synthetic promoter containing the ArcAB binding site of p_{lux}, which relieves inhibition by transcription factors ArcAB in the presence of the peroxide [41]).

The compound chemical reactions (transcription, translation, protein binding processing) underlying the proposed gene circuit are:

$$\emptyset \xrightarrow{\alpha_1 f_1(P)} L \xrightarrow{\gamma_1 g(L)} \emptyset$$

$$\emptyset \xrightarrow{\alpha_2 f_2(P)} H \xrightarrow{\gamma_2} \emptyset$$

$$\emptyset \xrightarrow{\alpha_3 f_3(H)} A \xrightarrow{\gamma_3} \emptyset$$

$$L + L_R \xrightarrow{k_1} P \xrightarrow{k_2} L + L_R$$

where L, H, A, L_R, P represent AHL, H_2O_2, Aiia, LuxR and the AHL-LuxR complex, respectively. Production is controlled by $f_i(Z) = (\delta_i + Z)/(c_i + Z)$, where $c_1 = k_{PL}$, $c_2 = k_{PH}$, $c_3 = k_{HA}$ are the thresholds for production of each species. Degradation is first order for H_2O_2 and Aiia, but enzymatic for AHL, with $g(L) = A/(k_{LD} + L)$. Total LuxR is assumed to be constant, and the AHL-LuxR complex (with relatively fast association and dissociation rates k_1, k_2) is assumed to be relatively stable to degradation.

Including mass-action dynamics of these reactions along with diffusion, and rescaling x by $D_L^{-1/2}$ such that $D = \frac{D_H}{D_L}$, results in the following equations,

$$\partial_t L = \alpha_1 \frac{\delta_1 + P}{k_{PL} + P} - \gamma_1 A \frac{L}{k_{LD} + L} - k_1(P_m - P)L + k_2 P + \nabla^2 L \tag{1}$$

$$\partial_t P = k_1(P_m - P)L - k_2 P \tag{2}$$

$$\partial_t H = \alpha_2 \frac{\delta_2 + P}{k_{PH} + P} - \gamma_2 H + D\nabla^2 H \tag{3}$$

$$\partial_t A = \alpha_3 \frac{\delta_3 + H}{k_{HA} + H} - \gamma_3 A \tag{4}$$

where P_m is the total amount of LuxR. The parameters of Eqs (1)–(4), and their nominal values used are listed in S1 Table.

Reducing Degradation Feedback Generates Limit Cycles and Turing Patterns

Restricting AiiA dynamics to reasonable relative production and degradation rates [26, 27], we find parameter regimes of stable fixed points, limit cycles, and Turing patterning. The maximal Aiia production rate, α_3, can be adjusted with plasmid copy number, ribosome binding site strength, or by using a hybrid promoter tuned with an inducer. Numerical analysis of the eigenvalues of the stable fixed point in Eqs (1)–(4) shows that slowing this maximal production rate leads to a stable limit cycle oscillation through a supercritical Hopf bifurcation, followed by a Turing instability, and a saddle node bifurcation (Fig 2a). The Turing instability bifurcation point is found by examining the characteristic equation,

$$|\mathbf{J} - \lambda\mathbf{I} - k^2\mathbf{D}| = 0 \tag{5}$$

for eigenvalues λ, where $\mathbf{J}$ is the Jacobian, $\mathbf{I}$ is the identity matrix, $\mathbf{D}$ is the matrix of diffusion coefficients, and k is the wavenumber. This equation is solved for different α_3, with the largest positive real parts of the eigenvalues plotted in Fig 2b. Having only two diffusable substances
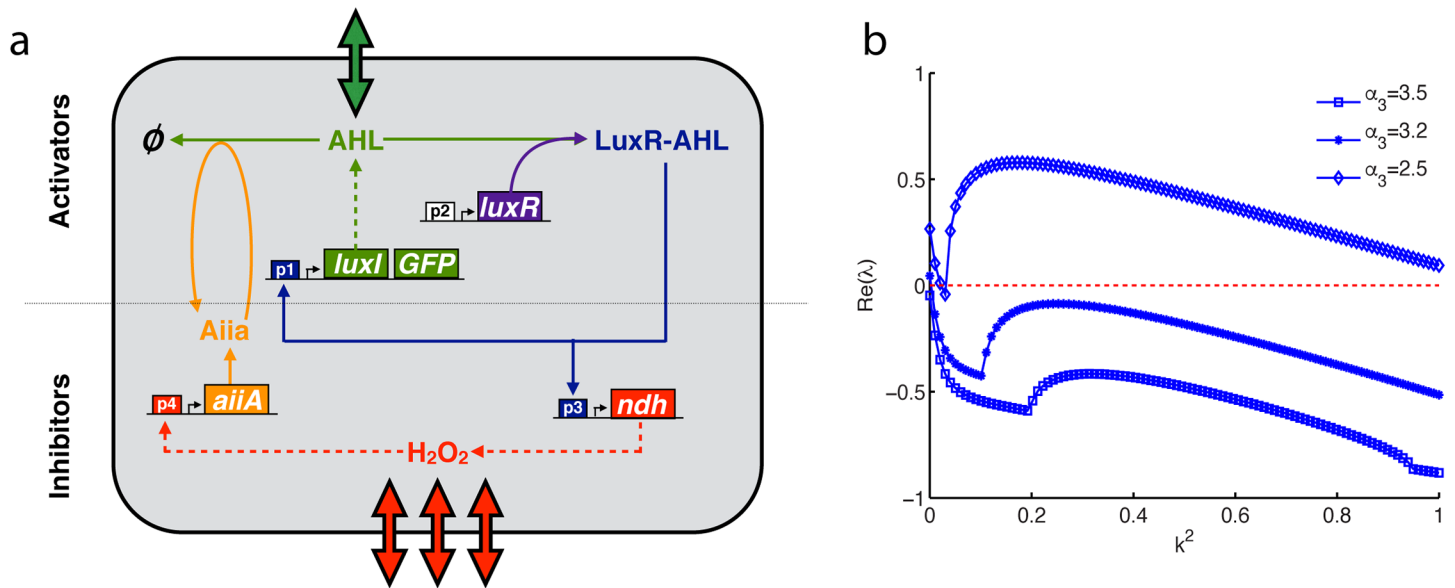
Fig 2. Slowing AiiA production in Eqs (1)–(4) leads to oscillations and Turing patterns. A codimension one bifurcation of the AHL fixed point, L_*, losing stability through a Hopf bifurcation and into a Turing instability as Aiia production rate is decreased. (b) Eigenvalue-wavenumber curves at various AiiA maximal production rates, corroborating the bifurcation analysis results above. At the cusp of each curve the eigenvalues become a complex conjugate pair, with each low eigenvalue left off the plot for clarity.

doi:10.1371/journal.pone.0153679.g002

leads to a quadratic equation in k^2, $A_{(\lambda)}(k^2)^2 + B_{(\lambda)}(k^2) + C_{(\lambda)} = 0$. Finding the root of the discriminant of the quadratic, $B_{(\lambda=0)}^2 - 4A_{(\lambda=0)}C_{(\lambda=0)}$, gives the condition for the Turing instability boundary ($\alpha_3 = 3.1$ min.$^{-1}$ in Fig 2a)).

Numerical simulations of the system in one spatial dimension with periodic boundary conditions further confirm a stable focus at $\alpha_3 = 3.5$ min.$^{-1}$ (Fig 3a), a stable limit cycle at $\alpha_3 = 3.2$ min.$^{-1}$ (Fig 3b), and Turing instability at $\alpha_3 = 2.5$ min.$^{-1}$ (Fig 3c). In two spatial dimensions the instability leads to formation of spot patterns (for snapshots of simulations with periodic boundary conditions, see Fig 3d, and for movies with no-flux boundary conditions, see S1 Movie). Our observation of Turing instability taking over from Hopf instability has previously seen in other systems [42–44]. Lowering the AiiA degradation rate (or the slowing of AiiA dynamics in general) leads to a similar sequence of transitions from a homogeneous steady state to temporal oscillations followed by Turing patterns, but this was not investigated in detail, as such parameters would be more difficult to control experimentally.

Overall, the results indicate that slowing AiiA feedback on AHL degradation can lead to limit cycle oscillations before the onset of Turing patterns. This is consistent with previous studies showing that an increased time delay in a negative feedback signal produces limit cycle oscillations [45–47]. It is interesting to note that for the cases shown in Fig 2, the fixed point is already unstable at $k = 0$ (a limit cycle) when undergoing the transition to the Turing instability. This means that the classic notion of Turing patterns arising from a stable fixed point can be extended to include some cases with an unstable point inside a limit cycle.
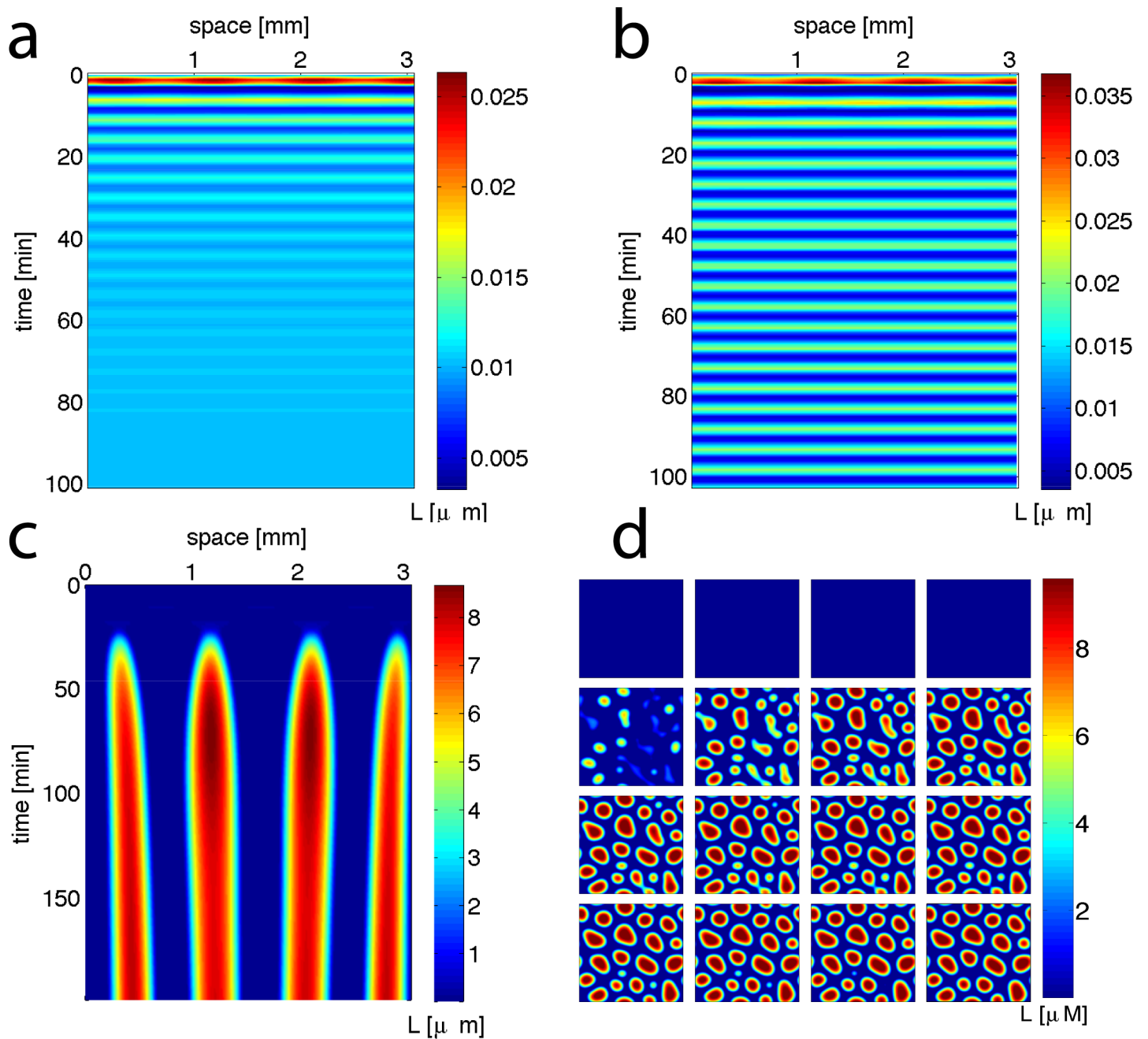
Fig 3. Numerical simulations of spatial dynamics in the model, Eqs (1)–(4), with periodic boundary conditions. (a-c) For 1-D space, slowing AiiA production confirms (a) stable focus at $\alpha_3 = 3.5$ min.$^{-1}$, (b) limit cycle at $\alpha_3 = 3.2$ min.$^{-1}$, and (c) Turing patterns at $\alpha_3 = 2.5$ min.$^{-1}$. (d) The same parameters as (c) lead to spot patterns in 2-D simulations with periodic boundary conditions (4.87×4.87 cm^2 panels taken every 13 mins).

doi:10.1371/journal.pone.0153679.g003

Controlling Range of Unstable Wavenumbers and Patterning Robustness

We next investigate how additional parameters can be used to experimentally tune spatial patterning in the circuit. In contrast to the single promoter circuit model that was proposed [30], increasing the cooperativity of transcriptional activation in our model does not appear to increase the parameter space leading to Turing patterns, since an increased rate of activation is not automatically balanced by an increased rate of repression. This however is not a major concern since increasing cooperativity would be challenging to implement in experiments.

A more experimentally tuneable parameter is α_1, affecting the maximal rate of LuxI expression, and experimentally controlled by a regulatable hybrid promoter, plasmid copy number, or the strength of the promoter or ribosome binding site. Covarying this parameter with the AiiA production rate creates basins for stable, Hopf unstable and Turing unstable solutions (Fig 4a). For $\alpha_3 < 0.16$ min.$^{-1}$ there is no α_1 that gives rise to Turing patterning. For the parameter space investigated (Fig 4a) as α_1 is increased, the range of α_3 leading to Turing patterning (α_3-robustness) also increases. Raising α_3 also tends to increase α_1-robustness (Fig 4a and 4b). Fig 4b demonstrates that raising the AiiA production rate expands the range of wavenumbers corresponding to the Turing instability, $Re(\lambda(k)) > 0$ towards higher wavenumbers (shorter wavelengths). Thus, tuning the maximal AiiA production rate to achieve more α_1-robust Turing patterning also results in shorter spatial periods in the resultant pattern.

Another parameter to control experimentally is P_m, representing the amount of LuxR. At the nominal parameter set (S1 Table), the Turing instability occurs for $P_m > 0.18$ (Fig 4c). Overall, the P_m-robustness of Turing patterning is not very sensitive to α_1, except near the borders of the Turing space (Fig 4c). Furthermore, the α_1-robustness of patterning is not much affected by increasing P_m (Fig 4c and 4d). It is clear however that a higher amount of LuxR leads to much shorter spatial periods in the Turing pattern (Fig 4d). Both codimension two bifurcation plots (Fig 4a and 4c) show that the Turing regime can be adjacent in parameter space to a regime of limit cycle dynamics (as in Fig 2), but this is not always the case (for example, decreasing α_1 when $0.5 < \alpha_3 < 3.2$, in Fig 4a).

Together these results show that Turing patterning with this circuit requires an AHL production rate high enough to prevent a stable focus or limit cycle, but not so high as to lose the fixed point through a saddle node bifurcation. Furthermore, it appears that the AiiA production rate is the highest-priority parameter to adjust in order to achieve Turing patterning that is robust to variations in the other experimental parameters. Once inside the Turing unstable regime, both LuxI production rate and the amount of LuxR can be used to tune the range of spatial periods in the solution.

Discussion

In this paper we have demonstrated the possibility of generating Turing patterns using a long-range gas signal that induces degradation of a short-range quorum sensing molecules. The next important step is to experimentally implement this proposed circuit in and test the predictions made by the model. The gene circuit has features in common with previous designs [26, 27], but there are some important differences. The Aiia promoter would likely need to be redesigned to be activated by exclusively by H_2O_2 instead of LuxR-AHL. Besides the use of *ndh*, H_2O_2 generation could also be increased by addition of a *lux*-induced *sodA* gene [27]. For the *lux*-like promoters (p_1 and p_3 in Fig 1), the model shows that they should be distinct from each other, with leak and maximal production from p_1 being higher than those from p_3 (compare $\delta_{1,2}$'s and $\alpha_{1,2}$'s in S1 Table). Alternatively, this could be achieved by putting ribosome binding sites on *luxI* that are stronger than those on *ndh*. It may also be necessary to remove the ArcAB sites on these
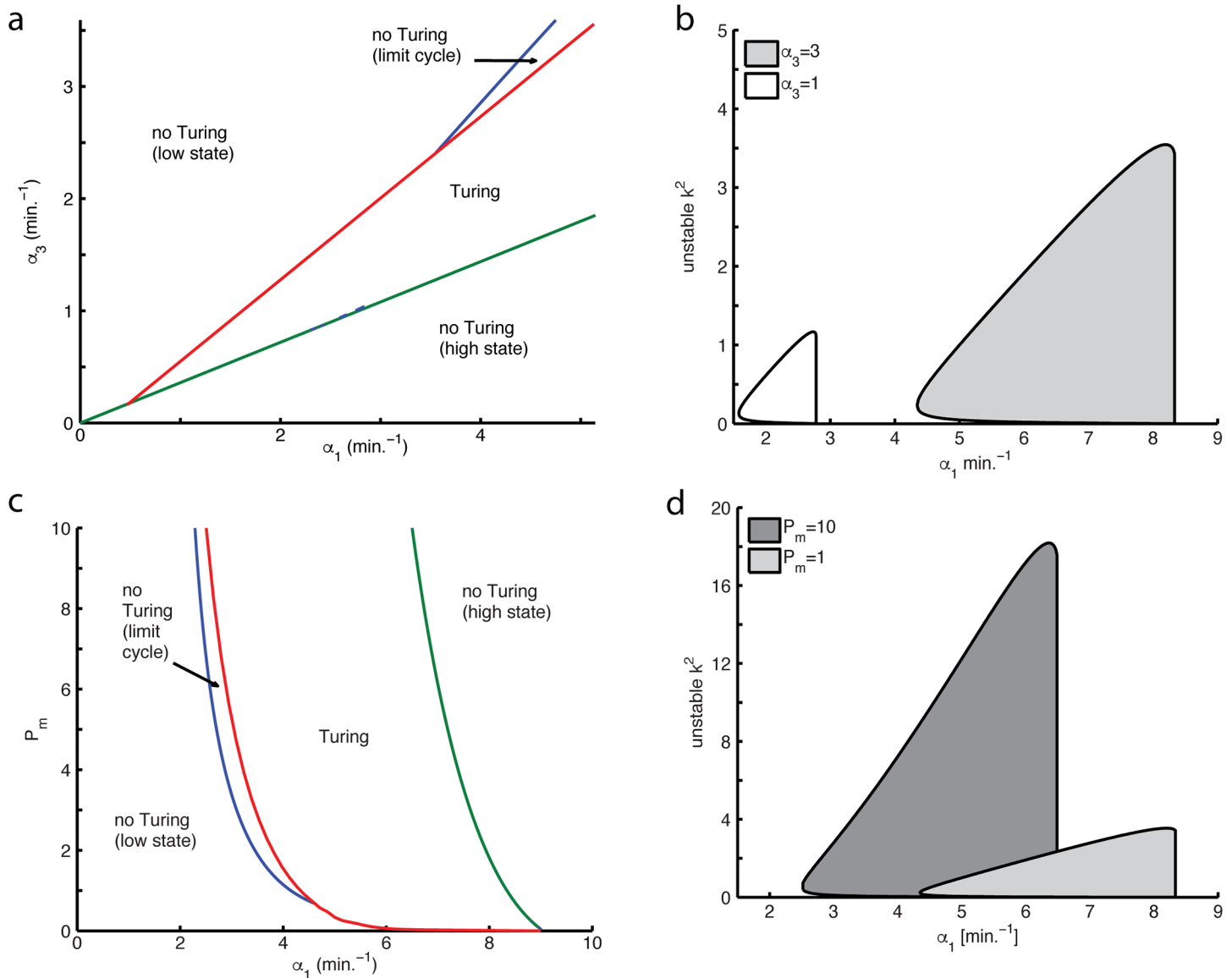
Fig 4. Dependence of Turing parameter space and wavenumbers on quorum sensing and AiiA parameters. (a,c) Two-parameter sections of Turing space, with curves of limit points (green), Hopf points (red), and Turing points (blue). (b,d) Ranges of Turing unstable wavenumbers for different sections along the maximal LuxI production rate within the Turing parameter space. Parameter values are varied from the nominal set (S1 Table).

doi:10.1371/journal.pone.0153679.g004

promoters to eliminate crosstalk with the H_2O_2 part of the circuit, but preliminary analysis shows that crosstalk as high as 20% can still lead to patterning (see S1 Equations) and S3 Fig. One could also consider using alternative quorum sensing systems [48] and volatile signaling molecules such as nitric oxide [49], ammonia [50], hydrogen sulfide [51], or ethylene [52].

Pattern formation speed is relevant to producing spatial structures in time scales allowed by experiments. This speed is reflected by the magnitude of $Re(\lambda) > 0$, that determines how fast unstable solutions diverge from the fixed point. Although the high dimensionality of our model makes it challenging to derive analytical expressions for the pattern formation speed (as

was done in [30, 53] for two-dimensional models), computing dispersion relations for different parameters demonstrates that pattern formation speed around the nominal parameter set is inversely related to α_3 (Fig 2b), but proportional to D (S1 Fig), α_1 and P_m (S2 Fig). Although pattern formation speed will typically be very slow near the transition to Turing instability, our simulations within the Turing parameter space demonstrate formation of patterns within two hours (Fig 3c and 3d), making the system quite accessible to experimental observation.

Bacteria engineered with this gene circuit could be tested on agar plates or inside microfluidic chambers, both of which are amenable to spatiotemporal data collection with an epifluorescence microscope. In one spatial dimension, one could use microfluidic devices like the long trap [26], or an annular trap [54] to study periodic boundary conditions. Agar could be patterned into one-dimensional spatial structures, but these are likely to exhaust nutrients or lose moisture too quickly. Spatial patterns in two dimensions are easier to generate on agar plates (as in [5, 23, 24]), because use of microfluidics would likely be complicated by diffusional anisotropies resulting from constant perfusion of liquid media through the channels. If this were not a challenge then one could exploit the gas-permeability of polydimethylsiloxane (commonly used to fabricate microfluidic devices) to allow for selective diffusion of H_2O_2 (as in [27]), or sequester the gas using vacuum channel in the microfluidic device (another use for the vacuum channel that was originally built for shear-free loading of cells [55]).

Another potential challenge to implementing these results experimentally arises from the assumptions made about diffusion. First, transport through and between the cells is only approximated by the diffusion equation. Limited membrane permeability and cell crowding can slow transport of signaling molecules, resulting in a smaller effective diffusion coefficient [56]. The effective diffusion coefficients of AHL and H_2O_2 have not been measured directly for bacterial monolayers in microfluidic devices. However, Danino and colleagues [26] measured conduction velocity of AHL-mediated activation to be $V = 8.5\text{-}35 \frac{\mu m}{min}$, which combined with the model prediction of $V = 0.17 D_L^{1/2}$, results in $D_L = 2.5\text{-}42 \times 10^3 \frac{\mu m^2}{min}$. This estimate is comparable to $D_L = 5.9\text{-}29 \times 10^3 \frac{\mu m^2}{min}$ (lower limit for biofilm; upper limit for water at 25°C) estimated by Stewart [56]. For H_2O_2, $D_H = 72\text{-}120 \times 10^3 \frac{\mu m^2}{min}$ [56], implying that the diffusion ratio, $D = 4\text{-}12$. However, Prindle *et al.* measured H_2O_2-mediated fluorescence conduction velocity $V \approx 700 \frac{\mu m}{min}$ across the biopixels microfluidic device [27], so using the 0.17 prefactor that Danino [26] found demonstrates that the ratio, $D = 100$, used in our model is reasonable. In addition, decreasing D as much as fourfold from $D = 100$ can still allow for patterning to occur (S1 Fig). If required, further disparity between gas and lactone diffusion could be attained by using crowding agents like polyethylene glycol, or engineering circuits with slower diffusing quorum sensing molecules [48].

The mathematical model presented could be further investigated by incorporating several additional layers of detail. This includes a more biophysical description of AHL production (LuxI catalyzes the conversion of SAM to AHL), as well as H_2O_2 production (NDH-2 catalyzes formation of H_2O_2), and regulation of the *aiiA* promoter (for example, H_2O_2 oxidizes ArcA to relieve repression of *lux* promoter [27]). All of these processes have been lumped together (represented by dashed arrows in Fig 1) in the current model, but may turn out to have a non-negligible effect on dynamics. Our model also lumps the processes transcription, translation and protein maturation. Thus it would also be interesting to include these processes and also compare this system to one reduced to a spatially-extended delay differential equation. Previous work [57, 58] suggested that delays can predispose that system to oscillatory patterning, which is consistent with what we found upon the inclusion of slower AiiA dynamics (Figs 2a and 4a). Another feature that the current model ignores is the effect of protein dilution due to cell growth. While this may hinder implementation in exponentially growing cells, there is also

work suggesting that an expanding domain can help make the Turing patterning regime more robust [57]. Furthermore, the dilution problem can be fundamentally resolved by engineering the chemical reactions in an *in vitro* transcription-translation system [59].

Considering that protein numbers are low at the steady states analyzed (the nanomolar range corresponds to tens of molecules per *E. coli*), it would be prudent to further examine this system using stochastic simulations. Hsia and colleagues [29] found that such stochastic effects changed the patterning parameter parameter space, but did not destroy the ability to produce Turing patterning. Although external fluctuations tend to destabilize the Turing parameter regime in a continuum setting [57], it has also been shown that when space is discrete, either intrinsic or extrinsic noise can cause patterning over larger parameter ranges [60, 61]. Testing these additional considerations is a good direction for future modeling studies.

Despite these theoretical and experimental challenges in further studying the proposed circuit we believe it is well worth the effort, as these types of gas and quorum sensing circuits could be quite useful for studies of bacterial morphogenesis and several synthetic biology applications. The present work provides a conceptual foundation and guidance for the development of gas mediated spatial patterning in multi-cellular and cell-free gene expression systems.

Supporting Information

S1 Table. Nominal parameter set.
(PDF)

S1 Fig. Effects of the diffusion coefficients ratio on the eigenvalue-wavenumber curves.
Dependence of the dispersion relation on the ratio of diffusion coefficients, D. (a) At the nominal parameter set (S1 Table) except with $\alpha_1 = 2.5$ and $\alpha_3 = 1.5$, the Turing instability persists for $D \geq 45$. (b) For $\alpha_3 = 2.5$, despite a Hopf instability at $k = 0$, Turing patterns are maintained when decreasing the ratio as low as $D = 25$.
(PDF)

S2 Fig. Effect of LuxI and LuxR parameter on the eigenvalue-wavenumber curves. Dependence of the dispersion relation on LuxI and LuxR parameters. Varying these parameters around the nominal parameter set (S1 Table) demonstrates that the pattern formation speed is proportional to both: (a) LuxI maximal production (α_1), and (b) amount of LuxR (P_m).
(PDF)

S1 Equations. The model incorporating the crosstalk between H_2O_2 and the p_{lux}-like promoters.
(PDF)

S3 Fig. Effects of H_2O_2 crosstalk with p_{lux} on the eigenvalue-wavenumber curves. Dispersion relations for the expanded model (S1 Equations), varying the relative effect H_2O_2 on p_{lux}, β. At the nominal parameter set (S1 Table) patterning still occurs with H_2O_2-p_{lux} crosstalk as high as 20%.
(PDF)

S1 Movie. Spot pattern formation with no-flux boundary conditions.
(MOV)

Acknowledgments

Author Contributions

Conceived and designed the experiments: BB LT. Performed the experiments: BB. Analyzed the data: BB JH LT. Contributed reagents/materials/analysis tools: JH LT. Wrote the paper: BB JH LT.

References

1. Grzybowski B, Bishop K, Campbell C, Fialkowski M, Smoukov S (2005) Micro- and nanotechnology via reaction-diffusion. Soft Matter 1: 114–128. doi: 10.1039/b501769f

2. Rassmi C, Kapral R (2009) Dynamics of Self-Organized and Self-Assembled Structures. Cambridge University Press, New York, 189–211 pp.

3. Stewart P (2008) Physiological heterogeneity in biofilms. Nature Reviews Microbiology 6: 199–210. doi: 10.1038/nrmicro1838 PMID: 18264116

4. V T, Øvreås L (2002) Microbial diversity and function in soil: from genes to ecosystems. Current Opinion in Microbiology 5: 240–245. doi: 10.1016/S1369-5274(02)00324-7

5. Liu C, Fu X, Liu L, Ren X, Chau C, et al. (2012) Sequential establishment of stripe patterns in an expanding cell population. Science 334: 238–241. doi: 10.1126/science.1209042

6. Asally M, Kittisopikul M, Rué P, Du YJ, Hu ZX, et al. (2012) Localized cell death focuses mechanical forces during 3d patterning in a biofilm. Proceedings of the National Academy of Sciences 109: 18891–18896. doi: 10.1073/pnas.1212429109

7. Davidson E, Erwin D (2006) Gene regulatory networks and the evolution of animal body plans. Science 311: 796–800. doi: 10.1126/science.1113832 PMID: 16469913

8. Morelli L, Uriu K, Ares S, Oates A (1997) Self-induced splitting of spiral-shaped spreading depression waves in chicken retina. Gene Regulatory Networks and the Evolution of Animal Body Plans 115: 319–324.

9. Economou A, Ohazama A, Porntaveetus T, Sharpe P, Kondo S, et al. (2012) Periodic stripe formation by a turing mechanism operating at growth zones in the mammalian palate. Nature Genetics 44: 348–351. doi: 10.1038/ng.1090 PMID: 22344222

10. Müller P, Rogers K, Jordan B, Lee J, Robson D, et al. (2012) Quorum sensing: cell-to-cell communication in bacteria. Science 336: 721–724. PMID: 16212498

11. Clément R, Mauroy B (2014) An archetypal mechanism for branching organogenesis. Physical Biology 11: 016003. doi: 10.1088/1478-3975/11/1/016003 PMID: 24442123

12. Turing A (1952) The chemical basis of morphogenesis. Philosophical Transactions of the Royal Society of London Series B, Biological Sciences 237: 473–480. doi: 10.1098/rstb.1952.0012

13. Murray J (1991) Mathematical Biology, Second Edition. Springer-Verlag, New York, 372–434 pp.

14. Sawai S, Maeda Y, Sawada Y (2000) Spontaneous symmetry breaking turing-type pattern formation in a confined *dictyostelium* cell mass. Physical Review Letters 85: 2212–2215. doi: 10.1103/PhysRevLett.85.2212 PMID: 10970500

15. Holloway D, Harrison L (2008) Pattern selection in plants: Coupling chemical dynamics to surface growth in three dimensions. Annals of Botany 101: 361–374. doi: 10.1093/aob/mcm295 PMID: 18045793

16. Smith R (2008) The role of auxin transport in plant patterning mechanisms. PLoS Biology 6: e323. doi: 10.1371/journal.pbio.0060323 PMID: 19090623

17. Marcon L, Sharpe J (2012) Turing patterns in development: what about the horse part? Current Opinion in Genetics & Development 22: 578–584. doi: 10.1016/j.gde.2012.11.013

18. Sheth R, Marcon L, Bastida M, Junco M, Quintana L, et al. (2012) Hox genes regulate digit patterning by controlling the wavelength of a turing-type mechanisms. Science 338: 1476–1480. doi: 10.1126/science.1226804 PMID: 23239739

19. Menshykau D, Dagmar Iber D (2013) Kidney branching morphogenesis under the control of a ligand–receptor-based turing mechanism. Physical Biology 10: 046003. doi: 10.1088/1478-3975/10/4/046003 PMID: 23770927

20. Nakamasu A, Takahashi G, Kanbe A, Kondo S (2009) Interactions between zebrafish pigment cells responsible for the generation of turing patterns. Proceedings of the National Academy of Sciences 106: 8429–8434. doi: 10.1073/pnas.0808622106

21. Lengyel I, Epstein I (1992) A chemical approach to designing turing patterns in reaction-diffusion systems. Proceedings of the National Academy of Sciences 89: 3977–3979. doi: 10.1073/pnas.89.9.3977

22. Bonnefont A, Varela H, Krischer K (2005) Stationary spatial patterns during bulk co electrooxidation on platinum. The Journal of Physical Chemistry B 109: 3408–3415. doi: 10.1021/jp045821v PMID: 16851372

23. Basu S, Gerchman Y, Collins C, Arnold F, Weiss R (2005) A synthetic multicellular system for programmed pattern formation. Nature 434: 1130–1134. doi: 10.1038/nature03461 PMID: 15858574

24. Payne S, Li B, Cao L, Schaeffer D, Ryser M, et al. (2013) Temporal control of self-organized pattern formation without morphogen gradients in bacteria. Molecular Systems Biology 9: 1–10.

25. Matsuda M, Koga M, Nishida E, Ebisuya M (2012) Synthetic signal propagation through direct cell-cell interaction. Science Signaling 5: ra31. doi: 10.1126/scisignal.2002764 PMID: 22510469

26. Danino T, Mondragón-Palomino O, Tsimring L, Hasty J (2010) A synchronized quorum of genetic clocks. Nature 463: 326–330. doi: 10.1038/nature08753 PMID: 20090747

27. Prindle A, Samayoa P, Razinkov I, Danino T, Tsimring L, et al. (2012) A sensing array of radically coupled genetic 'biopixels'. Nature 471: 39–44.

28. Schaerli Y, Munteanu A, Gili M, Cotterell J, Sharpe J, et al. (2014) A unified design space of synthetic stripe-forming networks. Nature communications 5. doi: 10.1038/ncomms5905 PMID: 25247316

29. Hsia J, Holtz W, Huang D, Arcak M, Maharbiz M (2012) A feedback quenched oscillator produces turing patterning with one diffuser. PLoS, Computatikonal Biology 8: e1002331. doi: 10.1371/journal.pcbi.1002331

30. Diambra L, Senthivel V, Menendez D, Isalan M (2015) Cooperativity to increase turing pattern space for synthetic biology. ACS Synthetic Biology 4: 177–186. doi: 10.1021/sb500233u PMID: 25122550

31. Lee H, DeLoache WC, Dueber JE (2012) Spatial organization of enzymes for metabolic engineering. Metabolic Engineering 14: 242–251. doi: 10.1016/j.ymben.2011.09.003 PMID: 21946160

32. Chiu D, Jeon N, Huang S, Kane R, Wargo C, et al. (2000) Patterned deposition of cells and proteins onto surfaces by using three-dimensional microfluidic systems. Proceedings of the National Academy of Sciences 97: 2408–2413. doi: 10.1073/pnas.040562297

33. Goldman D (2014) Regeneration, morphogenesis and self-organization. Development 141: 2745–2749. doi: 10.1242/dev.107839 PMID: 25005469

34. Chen H, Xu Z, Mei C, Yu D, Small S (2012) A system of repressor gradients spatially organizes the boundaries of bicoid-dependent target genes. Cell 149: 618–629. doi: 10.1016/j.cell.2012.03.018 PMID: 22541432

35. MATLAB (2012) version 8.1.0 (R2013a). Natick, Massachusetts: The MathWorks Inc.

36. Dhooge A, Govaerts W, Kuznetsov A (2004) Matcont: A matlab package for numerical bifurcation analysis of odes. ACM Transactions on Mathematical Software 29: 141–164. doi: 10.1145/779359.779362

37. Borek B, Shajahan TK, Gabriels J, Hodge A, Glass L, et al. (2012) Pacemaker interactions induce reentrant wave dynamics in engineered cardiac culture. Chaos 22: 033132. doi: 10.1063/1.4747709 PMID: 23020471

38. Dillon R, Maini P, Othmer H (1994) Pattern formation in generalized turing systems i. steady-state patterns in systems with mixed boundary conditions. Journal of Mathematical Biology 32: 345–393. doi: 10.1007/BF00160165

39. Liu D, Momb J, Thomas P, Moulin A, Petsko G, et al. (2008) Mechanism of the quorum-quenching lactonase (aiia) from bacillus thuringiensis. Biochemistry 47: 7706–7714. doi: 10.1021/bi800368y PMID: 18627129

40. Weinstein-Fischer D, Elgrably-Weiss M, Altuvia S (2000) Escherichia coli response to hydrogen peroxide: a role for dna supercoiling, topoisomerase i and fis. Molecular Microbiology 35: 1413–1420. doi: 10.1046/j.1365-2958.2000.01805.x PMID: 10760142

41. Georgellis D, Kwon O, Lin E (2001) Quinones as the redox signal for the arc two-component system of bacteria. Science 292: 2314–2316. doi: 10.1126/science.1059361 PMID: 11423658

42. Steyn-Ross M, Steyn-Ross D, Sleigh J (2013) Interacting turing-hopf instabilities drive symmetry-breaking transitions in a mean-field model of the cortex: A mechanism for the slow oscillation. Physical Review X 3: 021005. doi: 10.1103/PhysRevX.3.021005

43. Mincheva M, Roussel M (2012) Turing-hopf instability in biochemical reaction networks arising from pairs of subnetworks. Mathematical Biosciences 240: 1–11. doi: 10.1016/j.mbs.2012.05.007 PMID: 22698892

44. Baurmann M, Gross T, Feudel U (2007) Instabilities in spatially extended predator-prey systems: Spatio-temporal patterns in the neighborhood of turing-hopf bifurcations. Journal of Theoretical Biology 245: 220–229. doi: 10.1016/j.jtbi.2006.09.036 PMID: 17140604

45. Goodwin B (1965) Oscillatory behavior in enzymatic control processes. Advances in Enzyme Regulation 3: 516–519. doi: 10.1016/0065-2571(65)90067-1

46. Elowitz M, Leibler S (2000) A synthetic oscillatory network of transcriptional regulators. Nature 403: 335–338. doi: 10.1038/35002125 PMID: 10659856

47. Stricker J, Cookson S, Bennett M, Mather W, Tsimring L, et al. (2000) A fast, robust and tunable synthetic gene oscillator. Nature 456: 516–519. doi: 10.1038/nature07389

48. LaSarre B, Federle M (2013) Exploiting quorum sensing to confuse bacterial pathogens. Microbiology and Molecular Biology Reviews 77: 73–111. doi: 10.1128/MMBR.00046-12 PMID: 23471618

49. Archer E, Robinson A, Süel GM (2012) Engineered e. coli that detect and respond to gut inflammation through nitric oxide sensing. ACS Synthetic Biology 1: 451–457. doi: 10.1021/sb3000595 PMID: 23656184

50. Palková Z, Janderová B, Zikánová B, Pospí ek M, Forstová J (1997) Ammonia mediates communication between yeast colonies. Nature 390: 532–536. doi: 10.1038/37398 PMID: 9394006

51. Li L, Rose P, Moore P (2011) Hydrogen sulfide and cell signaling. Annual Review of Pharmacology and Toxicology 51: 169–187. doi: 10.1146/annurev-pharmtox-010510-100505 PMID: 21210746

52. Digiacomo F, Girelli G, Aor B, Marchioretti C, Pedrotti M, et al. (2014) Ethylene-producing bacteria that ripen fruit. ACS Synthetic Biology 3: 935–938. doi: 10.1021/sb5000077 PMID: 25393892

53. Miura T, Maini PK (2004) Speed of pattern appearance in reaction-diffusion models: implications in the pattern formation of limb bud mesenchyme cells. Bulletin of mathematical biology 66: 627–649. doi: 10.1016/j.bulm.2003.09.009 PMID: 15210310

54. Ferry M, Razinkov I, Hasty J (2011) Chapter fourteen–microfluidics for synthetic biology: From design to execution. In: Voigt C, editor, Synthetic Biology, Part A, Academic Press, volume 497 of *Methods in Enzymology*. pp. 295–372.

55. Kolnik M, Tsimring L, Hasty J (2012) Vacuum-assisted cell loading enables shear-free mammalian microfluidic culture. Lab Chip 12: 4732–4737. doi: 10.1039/c2lc40569e PMID: 22961584

56. Stewart P, Franklin M (2003) Diffusion in biofilms. Journal of Bacteriology 185: 1485–1491. doi: 10.1128/JB.185.5.1485-1491.2003 PMID: 12591863

57. Maini P, Woolley T, Baker R, Gaffney E, Lee S (2012) Turing's model for biological pattern formation and the robustness problem. Interface Focus 2: 487–496. doi: 10.1098/rsfs.2011.0113 PMID: 23919129

58. Gaffney E, Monk N (2006) Gene expression time delays and turing pattern formation systems. Bulletin of Mathematical Biology 68: 99–130. doi: 10.1007/s11538-006-9066-z PMID: 16794923

59. Noireaux V, Bar-Ziv R, Libchaber A (2003) Principles of cell-free genetic circuit assembly. Proceedings of the National Academy of Sciences 100: 12672–12677. doi: 10.1073/pnas.2135496100

60. Howard M, Rutenberg A (2003) Pattern formation inside bacteria: fluctuations due to the low copy number of proteins. Physical Review Letters 90: 12810. doi: 10.1103/PhysRevLett.90.128102

61. Butler T, Goldenfeld N (2011) Fluctuation driven turing patterns. Physical Review E 84: 011112. doi: 10.1103/PhysRevE.84.011112